
This is an electronic reprint of the original article.
This reprint may differ from the original in pagination and typographic detail.

Hentelä, Kristian; Kaario, Ossi; Garaniya, Vikram; Goldsworthy, Laurie; Larmi, Martti

A New Approach for Modeling Coke Particle Emissions from Large Diesel Engines Using Heavy Fuel Oil

Published in:

Proceedings of the SAE 2017 International Powertrains, Fuels and Lubricants Meeting

DOI:

[10.4271/2017-01-2381](https://doi.org/10.4271/2017-01-2381)

Published: 01/01/2017

Document Version

Peer-reviewed accepted author manuscript, also known as Final accepted manuscript or Post-print

Please cite the original version:

Hentelä, K., Kaario, O., Garaniya, V., Goldsworthy, L., & Larmi, M. (2017). A New Approach for Modeling Coke Particle Emissions from Large Diesel Engines Using Heavy Fuel Oil. In *Proceedings of the SAE 2017 International Powertrains, Fuels and Lubricants Meeting* (Vol. 2017-October). Article 2017-01-2381 (SAE Technical Papers). SAE International. <https://doi.org/10.4271/2017-01-2381>

This material is protected by copyright and other intellectual property rights, and duplication or sale of all or part of any of the repository collections is not permitted, except that material may be duplicated by you for your research use or educational purposes in electronic or print form. You must obtain permission for any other use. Electronic or print copies may not be offered, whether for sale or otherwise to anyone who is not an authorised user.

A new approach for modeling coke particle emissions from large diesel engines using heavy fuel oil

Kristian Hentelä
Gasmet Europe Oy

Ossi Kaario, Martti Larmi
Aalto University

Vikram Garaniya, Laurie Goldsworthy
University of Tasmania

Copyright © 1999 Society of Automotive Engineers, Inc.

ABSTRACT

In the present study, a new approach for modelling emissions of coke particles or cenospheres from large diesel engines using HFO (Heavy fuel oil) was studied. The model used is based on a multicomponent droplet mass transfer and properties model that uses a continuous thermodynamics approach to model the complex composition of the HFO fuel and the resulting evaporation behavior of the fuel droplets. Cenospheres are modelled as the residue left in the fuel droplets towards the end of the simulation. The mass-transfer and fuel properties models were implemented into a cylinder section model based on the Wärtsilä W20 engine in the CFD-code Star CD v.4.24. Different submodels and corresponding parameters were tuned to match experimental data of cylinder pressures available from Wärtsilä for the studied cases. The results obtained from the present model were compared to experimental results found in the literature. The performance of the model was found to be promising although conclusive validation of the model would require more detailed experimental results about cenosphere emissions from the specific case studied here. According to the results obtained from this model the emissions of cenospheres are a function of both operating conditions and fuel properties. While the droplet evaporation and properties models were used in this study to model cenosphere emissions, the approach could also be used to study the combustion behavior of HFO in a broader sense.

INTRODUCTION

Despite ever tightening restrictions on emissions and emerging alternative fuels, Heavy Fuel Oil (HFO) will still remain an important fuel for the foreseeable future, especially within the maritime transport industry[1], [2]. While the market share of HFO might decrease over time, from

about 80 % in 2010 due to the emergence of alternative fuels, Lloyds Register Marine still forecasts the share of HFO in the marine fuel market in 2030 to be between 47 % and 66 % [1]. With the increase in fuel demand this means that the total consumption of HFO is actually likely to increase in the near future.

This continuing prevalence of HFO as a transport fuel coupled with tightening environmental regulations means that there will be a demand for emissions abatement solutions for HFO combustion processes [2]. Additionally optimization of HFO combustion process is also useful for minimizing the challenges presented by using heavy fuels in large diesel engines. One challenge presented by using heavy fuel in an engine is the different behaviour with regards to emissions of particulate matter (PM) compared to operation with lighter fuels. PM emissions modelling in diesel combustion processes is generally focused on modelling soot particles formed in gas phase reactions between fuel molecules. Although this may give an accurate estimate when modelling emissions from operation with light distillate fuels, in combustion of HFO other mechanisms of PM formation are prevalent and gas phase soot presents only a fraction of total PM. The larger amount of impurities in HFO leads to larger emissions of ash and sulphates. In addition to this, the poorly evaporating heavy molecules present in HFO can lead to the formation of carbonaceous residue directly from the fuel droplets. While the ash emissions are easily estimated from the ash content in the fuel, predicting the emissions of the carbonaceous particles formed from the fuel droplets, commonly referred to as cenospheres, is more complicated.

According to Ikegami et al. [3] the combustion process of an HFO droplet consists of two distinct phases, a liquid droplet phase and a solid coke particle phase. First

comes the liquid droplet phase where the droplet turns into a solid coke particle through various heat- and mass-transfer processes. This phase can be seen as comprising the following four stages:

- Pre-ignition heating
- Evaporation
- Thermal decomposition
- Polymerisation

In short the droplet first heats up leading to the evaporation of lighter components in the droplet in order of their volatility. As the temperature rises, thermal cracking starts to take place and heavy molecules break down into lighter compounds which then evaporate. Lastly a process of polymerisation starts to take place, combining lighter molecules into polymer and thus solidifying the droplet into a coke particle. This begins the solid coke particle phase where the coke particle formed in the previous phase burns through surface oxidation. Essentially every fuel droplet will become a coke particle that is then consumed through surface oxidation [4].

While a considerable part of combustion modelling studies have focused on modelling distillate fuels there have also been attempts to model the complex behaviour of HFO described above. Most notably in this context Garaniya [5] proposed the model that is implemented into diesel combustion and emissions modelling in this study. Garaniya's work was influenced partly by the work of Baert, who proposed a droplet evaporation and pyrolysis model using four components to represent the composition of HFO [6]. While the evaporation modelling in Garaniya's model is different from Baert's, the droplet pyrolysis and polymerisation model was modified from the pyrolysis model of Baert.

Goldsworthy [7] has developed an HFO combustion and ignition model in the context of marine diesel engines. Goldsworthy used two components, cutter stock and residue, to model the properties of HFO [7]. Goldsworthy's model is however not suited for modelling coke particle emissions as the formation of carbonaceous residue in the droplets is not modelled apart from raising the critical temperature of the droplet to allow it to stay in the simulation. Struckmeier [8] elaborated on Goldsworthy's work adding a two component evaporation model, and Kyriakides [9] also developed an HFO model based on a similar two component approximation of the fuel. These models also do not address the issue of coke formation in the liquid phase.

The coke particles produced in HFO combustion will, given the right conditions, eventually be consumed completely. However, if there is not sufficient oxygen or time for this they will exit the process as PM emissions. High aromatic content in the fuel seems to be correlated with coke or cenosphere formation and cenosphere emissions

are associated with fuels with high asphaltene contents [5], [10]. However, predicting cenosphere emissions based on fuel properties alone seems problematic as there are studies contradicting direct correlations between asphaltene content and cenosphere emissions [4], [11]. Marrone et al. [11] found coke formation even with fuels where asphaltenes had been removed, and thus prediction of coke formation purely based on asphaltene content is problematic. Therefore the modelling approach used in this study could provide useful information on conditions leading to cenosphere emissions.

Additional approaches to modelling cenosphere formation were developed by Antaki [12], Lee et al. [13], Moszkowicz et al. [14] and Youan et al. [15]. The models of Antaki, Lee and Moszkowicz all assume that cenospheres are hollow spheres with a shell of coke. In all these models the formation of the hollow sphere is modelled by assuming that the coke formed as residue of the combustion process is gathered at the surface of the droplet forming a rigid porous shell. The liquid then evaporates through the shell thus thickening the shell and finally leaving the sphere hollow. In Antaki's model the droplet is assumed to form a cenosphere the same size as the original droplet, while in the models of Lee and Moszkowicz the size of the cenosphere is governed by a critical shell thickness [16]. The most recent model found in the literature was developed by Reddy et al. [16]. In the model of Reddy et al. [16] the formation of cenospheres is modelled in three stages; regression, shell formation and hardening and flow through rigid shell. In contrast to the models of Lee and Moszkowicz the size of the resulting cenospheres is not governed by an assumed critical value for shell thickness. Instead the critical value of cenosphere diameter is modelled through the balance of the pressures created by vapour flowing through the shell and the pressure on the shell due to the van der Waals energy of the coke layers and the surface energy [16]. One problem with implementing models such as the one by Reddy et al. [16] for modelling in medium speed diesel engines is that the model was validated for quite large droplet sizes. The model of Reddy et al. [16] was validated against experimental data for droplets with sizes of 490, 640 and 690 μm . These droplet sizes are quite large compared to those observed in spray studies for HFO in marine diesel engines [17].

Urban et al. [18] found that the amount of a given fuel oil that is converted into cenospheres is mainly a function of fuel properties and is fairly constant over a range of different operating conditions. They developed a measure for this called the CFI (Coke Formation Index) and speculated that it could be used to predict coke production in cases where droplet size distributions in the spray and the CFI of the fuel are known [18]. The CFI is essentially a simple empirical approach to modelling coke formation.

The purpose of this paper is to model and study the formation of carbonaceous particles from the fuel droplets in

HFO combustion in a diesel engine. Through modelling the emissions of PM this paper hopes to provide a tool for predicting PM emissions from HFO combustion as well as providing insight into the formation of these emissions. Understanding the mechanisms of formation and consumption of PM emissions is essential when developing engines in order to diminish these emissions. In this paper a new model for predicting cenosphere emissions is presented. The results from the model are compared to existing data of engine emissions and the performance of the model is evaluated

RESEARCH MATERIAL AND METHODS

The present study is based on the droplet evaporation and droplet properties models developed by Garaniya[5] and presented in his thesis titled "Modelling of Heavy Fuel Oil Combustion using Continuous Thermodynamics".[5] The model was developed to be used with the CFD-program Star-CD and is implemented into Star-CD with user subroutines using Fortran coding. The two main user subroutines that are used to implement the model are the subroutines drmast.f and droprof.f found in Star CD. These subroutines allow the specification of custom mass transfer processes for droplets and droplet properties. The model was originally developed for Star-CD v3.24 but the subroutines were updated in order to be compatible with the newer v4.24 which was used in the present study. In the following sections the model and the theory behind it are described. Details about its implementation into the Star-CD CFD code are also given along with an explanation of how the model can be applied to PM emissions modelling. Since there are many other submodels involved in the complete combustion model the choices of the most important submodels and the settings for these models in Star CD are also presented in order to give a complete understanding of the whole CFD model used for this work.

THE PRESENT MODEL The idea behind the present model is to use continuous thermodynamics in order to represent the complex composition of HFO. This allows the model to consider the composition of the fuel when calculating the mass transfer processes from the fuel droplets, without using excessive amounts of computational resources.

As discussed in earlier sections HFO contains such a large range of different hydrocarbons with varying structures and molecular weights, that modelling each of them as discrete components would not be practical.[5] Garaniya's droplet evaporation model solves this issue by using continuous thermodynamics to describe the composition instead of attempting to model each individual component in the fuel. This reduces the computational load while still managing to capture the behaviour of complex fuels. In continuous thermodynamics the fuel mixture composition is represented using Probability Density

Functions(PDF) of a characterizing variable. This characterizing variable is then used to predict other properties of the component. In the present model the molecular weight of the components is chosen as the characterizing variable, and the changes in other properties are modelled according to the change in the molecular weights of the components. In the present model the composition of the fuel is described by using four different components, each of which uses a PDF to describe a range of similar hydrocarbons. Three of the components describe lighter components in HFO that originate mainly from the cutter stock and the final component describes the heavy molecules that come from the fraction of heavy Residue in the fuel. The components used in this model are:

- N-Paraffins
- Aromatics
- Naphtenes
- Residue

The distribution of the molecular weights within these components is described using a distribution function. In the present model a Γ -distribution function(Schultz or Pearson type III function) is used. The choice of the Γ -distribution instead of the common Gaussian distribution is due to the fact that the Gaussian distribution is unbound at both ends and does not therefore lend itself well to cases where the characterizing variable requires a lower bound[5]. The Γ -distribution can be given as

$$F_j(I) = \frac{(I - \gamma_j)^{\alpha_j - 1}}{\beta_j^{\alpha_j} \Gamma(\alpha_j)} \exp\left(-\frac{(I - \gamma_j)}{\beta_j}\right) \quad (1)$$

where I is the characterizing variable, α_j and β_j , are shape parameters for the function and γ_j is the distribution origin. Both α_j and β_j in this model are different for the liquid phase and the vapour phase while γ_j is assumed to be the same in both phases. The mean and variance of this distribution for the liquid phase are given as

$$\theta_{Lj} = \alpha_{Lj} \beta_{Lj} + \gamma_j \quad (2)$$

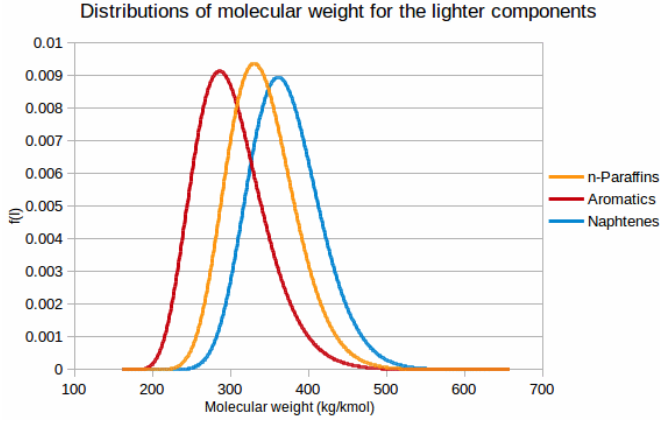
$$\sigma_{Lj}^2 = \alpha_{Lj} \beta_{Lj}^2 \quad (3)$$

where θ_{Lj} is the mean and σ_{Lj}^2 is the variance. The distribution parameters used for the different components in the beginning of the simulation are summarized in table 1[5]. The shape of the distributions corresponding to the

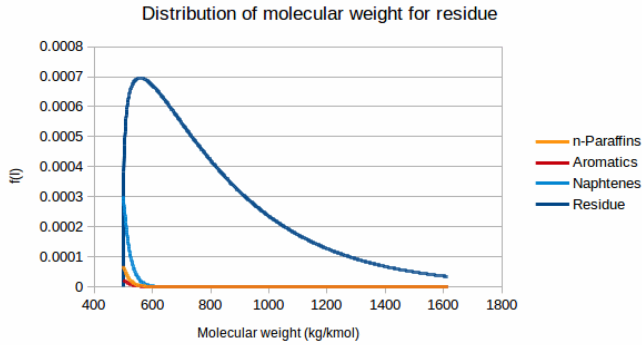
Table 1: Distribution parameters for Γ distribution

Components	Distribution Origin (γ)	Distribution mean (θ)	Standard deviation (σ)
1. n-Paraffins	160	340.00	43.69
2. Aromatics	160	300.00	45.75
3. Naphtenes	160	370.00	45.47
4. Residue	500	850.00	320.15

distribution parameters in Table 1 are presented in Figure 1. As the droplets are injected into the cylinder they will undergo mass transfer processes and the distribution



(a) Lighter components



(b) Residue

Figure 1: The PDF:s of the molecular weights of the different components at the beginning of simulations

parameters change during the simulation to account for the fact that the lightest components within each of the four fractions evaporate first. In the present model the mass transfer from the three lighter fractions is assumed to happen only through evaporation and the residue fraction is assumed not to evaporate, but to go through pyrolysis instead. After pyrolysis is complete, the pyrolysis residue will burn through heterogeneous surface oxidation. The mass transfer processes modelled in the present model are illustrated in figure 2. In the following subsections explanations are given for how the different processes illustrated in figure 2 are modelled with the present model. In order to keep the explanation of the model clear and concise the derivation of some equations is not explained in detail. For detailed theoretical explanations about the model readers should consult the original work by Garaniya on the development of the model.[5]

Evaporation Evaporation from the droplet surface is modelled through determining the Vapour-Liquid Equilibrium (VLE) at the droplets surface. As the VLE determines the concentration of vapour at the droplet surface it can be used to determine the evaporation of a component from the surface. The formulation of the VLE stems from the assumption that the chemical potential μ is the same for each phase at the boundary between phases. This can

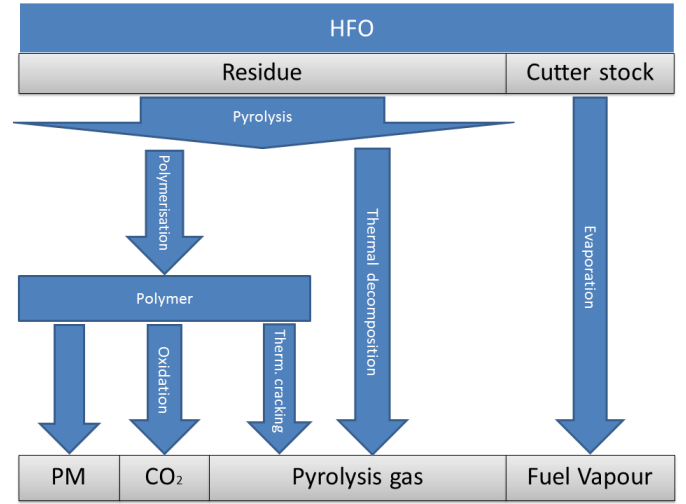


Figure 2: The mass transfer processes modelled in the present model

be stated as[5]

$$\mu_i^G = \mu_i^L \quad \text{for } i = 1, 2, 3 \dots s \quad (4)$$

where s is the total number of species. To describe the evaporation of a fuel consisting of such a large number of species as HFO would then include solving a huge number of chemical potential equations. Here continuous thermodynamics can significantly lower computational cost as an equation only needs to be solved for each component class, of which there are only four in the present model. The VLE formulation used in the present model is the low-pressure VLE model used by Garaniya [5]. This formulation makes the assumption that the vapour phase can be approximated as an ideal gas. The VLE can then be expressed using Raoult's law and formulated for component j using continuous thermodynamics as

$$y_{Fj} f_{Vj}(I) P = x_{Lj} f_{Lj}(I) P_j^{sat}(T, I) \quad (5)$$

where y_{Fj} is the vapour phase mole fraction of component j , x_{Lj} is the liquid phase mole fraction of component j , $f_{Lj}(I)$ and $f_{Vj}(I)$ are the liquid and vapour phase distributions for the molecular weight and $P_j^{sat}(T, I)$ is the vapour pressure of the component. The correlation in eq.5 can be used to solve the vapour phase mole fraction at the droplets surface y_{FjR} and the distribution parameters, mean molecular weight Θ_{jR} and variance σ_{jR}^2 , describing the fractions composition. Using the Clausius-Clapeyron equation to determine the vapour pressure of the component y_{FjR} , Θ_{jR} and σ_{jR}^2 are given as

$$y_{FjR} = \frac{\frac{P_{atm}}{P_\infty} \cdot \exp\left(\left(\frac{S_{fj}}{R_{GC}T_R}\right)(T_R - a_B - \gamma_j b_B)\right)}{\left(1 + \frac{S_{fj}}{R_{GC}T_R} b_B \beta_{Lj}\right)^{(\alpha_{Lj})}} \quad (6)$$

$$\theta_{jR} = \gamma_j + \frac{\theta_{Lj} - \gamma_j}{1 + \left(\left(\frac{S_{fj} b_b}{R_{GC}T_R} \frac{\sigma_{Lj}^2}{\theta_{Lj} - \gamma_j}\right)\right)} \quad (7)$$

and,

$$\sigma_{jR}^2 = \sigma_{Lj}^2 \left(\frac{\theta_{jR} - \gamma_j}{\theta_{Lj} - \gamma_j}\right)^2 \quad (8)$$

The total molar flux of vapour from the droplet is denoted as N . This is the sum of the molar fluxes caused by each of the components and ξ_j is the share of N that is caused by a single component. The ξ_j 's of each component are calculated as

$$\xi_j = \frac{y_{FjR} - y_{Fj\infty}}{\exp(2NR/cD_j Sh_0) - 1} \quad (9)$$

where c is the molar density, D_j is the average diffusivity of the component and $y_{Fj\infty}$ is the vapour phase mole fraction of component j far from the droplet. Sh_0 in eq. 9 is the Sherwood number and it is given as a constant $Sh_0 = 2$ as the droplet is stationary during the calculation of a single droplet. The total molar flux N and the molar flux fractions for each component have to be solved simultaneously to calculate the value of ξ_j and N . As species with light molecular weight evaporate first and leave the liquid phase, the distribution of molecular weights for each component changes. The mean molecular weight increases and the variance decreases. As component j evaporates with a fraction ξ_j of the total molar flux N the corresponding change of mean molecular weight is

$$d\theta_{Lj} = \frac{dt \cdot 3N}{x_{Lj} c_L R} \left(\theta_{Lj} \xi_j + \frac{\theta_{j\infty} y_{Fj\infty} - \theta_{jR} y_{Fjr} (1 + B_j)}{B_j} \right) \quad (10)$$

The change in the second central moment of the distribution $\psi_{Lj} = \theta_{Lj}^2 + \sigma_{Lj}^2$ can be calculated as

$$d\psi_{Lj} = \frac{dt \cdot 3N}{x_{Lj} c_L R} \left(\psi_{Lj} \xi_j + \frac{\psi_{j\infty} y_{Fj\infty} - \psi_{jR} y_{Fjr} (1 + B_j)}{B_j} \right) \quad (11)$$

B_j in equations 10 and 11 is given as

$$B_j = \frac{y_{FjR} - y_{Fj\infty}}{\xi_j - y_{FjR}} \quad (12)$$

The rate of evaporation of each component is then given as

$$\frac{dm_{Vj}}{dt} = -N \xi_j A \theta_{jR} \quad (13)$$

where A is the surface area of the droplet.

Pyrolysis As stated earlier the Residue component is assumed not to evaporate in the present model. The mass transfer processes from this component are assumed to happen only through pyrolysis. The processes involved in the pyrolysis of the residue fraction of the fuel, and modelled in the present work, are presented in Figure 2. The chemical bonds in the heavy molecules are broken due to the influence of high temperatures producing radicals. These radicals then either decompose and become lower molecular weight gases, or recombine through polymerisation producing coke residue. Polymerisation and thermal cracking occur simultaneously and non-aromatic part of formed polymer can also decompose through cracking. Thus both the thermal cracking and polymerisation have a dependence on both temperature and the aromaticity of the fuel (AR).[5]

The pyrolysis model in the present work is based on

the work of Baert with modifications to some model parameters[6]. The rate of pyrolysis gas production from the thermal cracking of liquid and polymer is given as

$$\frac{dm_G}{dt} = (m_{component} + m_{polymer}) \left(k_1 \exp\left(\frac{-E_1}{R_G C T}\right) (1 - AR) \right) \quad (14)$$

The rate of polymerisation is given as

$$\begin{aligned} \frac{dm_{Pj}}{dt} = & -m_{Pj} \left(k_1 \exp\left(\frac{-E_1}{R_G C T}\right) (1 - AR) \right) \\ & + m_{Lj} \left(\left(k_2 \exp\left(\frac{-E_2}{R_G C T}\right) \right) \right) \\ & + k_3 \exp\left(\frac{-E_3}{R_G C T}\right) AR \end{aligned} \quad (15)$$

Only the non-aromatic molecules exit the liquid phase through thermal cracking and this leaves only the aromatic fraction of the fuel in the liquid phase. This leads to an increase in the aromaticity of the liquid phase which is given as

$$\frac{dAR}{dt} = k_1 \exp\left(\frac{-E_1}{R_G C T}\right) (1 - AR) AR \quad (16)$$

The coefficients used in equations 14, 15 and 16 are presented in table 2. As stated earlier the pyrolysis model used here is based on the work of Baert. Garaniya used the same model but with modified parameters and further adjustments have been made to the parameters in the present work. The parameters used in Garaniya's work resulted in combustion behaviour that did not match the experimental pressure data available from the kind of engine modeled in this work. As the fuel used in Garaniya's tests and the experimental data available for this work was not the same, some adjustment of the parameters to achieve better combustion behaviour can easily be justified.

Table 2: Coefficients used for the pyrolysis model in this model as well as the works of Baert[6] and Garaniya[5]

Coefficients	Baert's model	Garaniyas modified model	Present model
k_1 (1/s)	2E7	8E7	16E10
k_2 (1/s)	8E6	5E7	5E7
k_3 (1/s)	1E13	1E13	1E13
E_1 (kJ/mol)	125E3	85E3	85E3
E_2 (kJ/mol)	100E3	90E3	90E3
E_3 (kJ/mol)	270E3	270E3	270E3

Polymer oxidation When most of the volatile compounds present in the beginning have left the droplet through evaporation and pyrolysis, the carbonaceous residue that was created through polymerisation, will start to oxidise. This is known as the polymer burnout phase. In the present model the burnout of polymer is modelled in a process analogous to the char burnout model in Star-CD. The polymer burnout phase in the present model is allowed to begin once the aromaticity of the droplet has reached 0.9 and 95 % droplet has been converted into polymer.

Similarly to the combustion model, the burnout of polymer is controlled by a combined rate coefficient. The combined rate is a combination of the diffusion rate and the

chemical rate and the burnout of polymer can be controlled by either one of these. The diffusion rate coefficient can be given as

$$K_d = 5.06 \cdot 10^{-12} \frac{T_{ref}^{0.75}}{d} \quad (17)$$

where T_{ref} is the reference temperature and d is the droplets diameter. The chemical rate coefficient can be given as

$$K_c = A_{poly} \exp\left(\frac{-E_{poly}}{R_G C T}\right) \quad (18)$$

where A_{poly} is the pre exponential factor for polymer E_{poly} is the activation energy for polymer. The value used for A_{poly} in the present model is $1.3 \text{ kgm}^{-2} \text{ s}^{-1} (\text{Nm}^{-2})^{-n}$ and the value for E_{poly} is $9.27 \cdot 10^7 \text{ J/kmol}$. The combined rate coefficient is then calculated as

$$q = \left(\frac{K_c K_d}{K_c + K_d}\right) P_g \quad (19)$$

where P_g is the partial pressure of oxygen in the surrounding medium. The rate of polymer burnout is dependent on the rate coefficient as well as the surface area of the droplet and can be calculated as

$$\frac{dPoly}{dt} = q \pi d^2 \quad (20)$$

Droplet properties As the lighter species evaporate from the droplet and its composition thus changes, some of the droplets properties will also change. The enthalpy of evaporation for each of the components, h_{fgj} , is given as;

$$h_{fgj} = \frac{T Y_j \Phi_{Hj}}{\theta_{Lj}} \quad (21)$$

where

$$T Y_j = a_j + (b_j / B_j) * (\theta_{jR} y_{FjR} (1 + B_j) - \theta_{\infty} y_{fj\infty}) \quad (22)$$

and

$$\Phi_{Hj} = (T_{CRj} - T)^{0.38} / c_j \quad (23)$$

The constants a_j , b_j and c_j in equations 22 and 23 are constants that differ for each of the components. The critical temperature of the component T_{CRj} is given as;

$$T_{CRj} = a_{crj} + (b_{crj} \theta_{jR}) \quad (24)$$

where a_{crj} and b_{crj} are again component specific constants. To get the heat of evaporation for the Residue fraction that evaporates only through pyrolysis the heat of decomposition $h_d = 4.0e7 \cdot \text{EXP}(-2.7 \cdot T_C / T_D)$ is added to the enthalpy of evaporation. Finally the specific heat of the liquid phase for each component, C_{pLj} , is calculated as

$$C_{pLj} = 1000(a_{cp} - (b_{cp} T_D) + (c_{cp} T_D^2)) \quad (25)$$

where a_{cp} , b_{cp} and c_{cp} are component specific constants. Viscosity and the surface tension coefficient are kept constant at values of 0.0135 kg/ms and 0.04 N/m respectively[5].

Application to modelling Cenosphere emissions The focus of this work is to model emissions of cenospheres. However, the model described above is not designed for the sole purpose of doing this and does not contain a single term that would describe emissions. It simply models all the mass transfer processes that take place for each droplet. The possibility to use this kind of a model to simulate cenosphere emissions is due to the fact that cenospheres are what is left of the fuel droplets once all the mass transfer processes have taken place. In the absence of sufficient oxygen or time for complete oxidation of the polymer through the polymer burnout phase, the polymer that is left will be emitted from the process as cenospheres. By looking at what is left of the droplets at the end of the simulation it is therefore possible to apply this model to simulating cenosphere emissions.

IMPLEMENTATION INTO STAR CD As the present model does not simply create a passive soot scalar that does not influence the other sub-models in the simulation, this mass-transfer sub-model cannot simply be added to a functioning model without consideration of its effects on the simulation as a whole. Many sub-models that are important in spray combustion need to be considered and optimized in order for the whole combustion model to work properly. In the following subsections some of the most important sub-models influencing the performance of the simulations are presented and the choice of models and parameters are motivated.

Computational Grid The computational grid used for the simulations in this study was developed by Kaario[19]. It is a sectional model representing a section of the cylinder in the Wartsila W20 engine. The mesh used in the model consists of 185665 cells and it is a moving mesh configuration where layers of cells deform and are collapsed and re-activated to model the movement of the piston. Figure 3 shows the computational grid at two different time steps.

Combustion and ignition The Laminar and Turbulent Characteristic Time combustion model(LaTCT), introduced by Abraham et al. [20] was used to model combustion along with the shell auto-ignition model, a combination which was first introduced to diesel engine modeling by Kong et al.[21]. The standard shell auto-ignition model parameters in Star-CD were used apart from the time-range when the model was active. The start time for ignition was set to match experimental data for each load case and the end time was set to a point late in the cycle to allow model conditions to determine when ignition occurs. The LaTCT combustion model was implemented into Star-CD using a user-subroutine developed by Kaario[19]. In the LaTCT combustion model the combustion rate is determined by a combination of chemical and turbulent time-scales. The characteristic time that combines the two aforementioned time-scales is given as

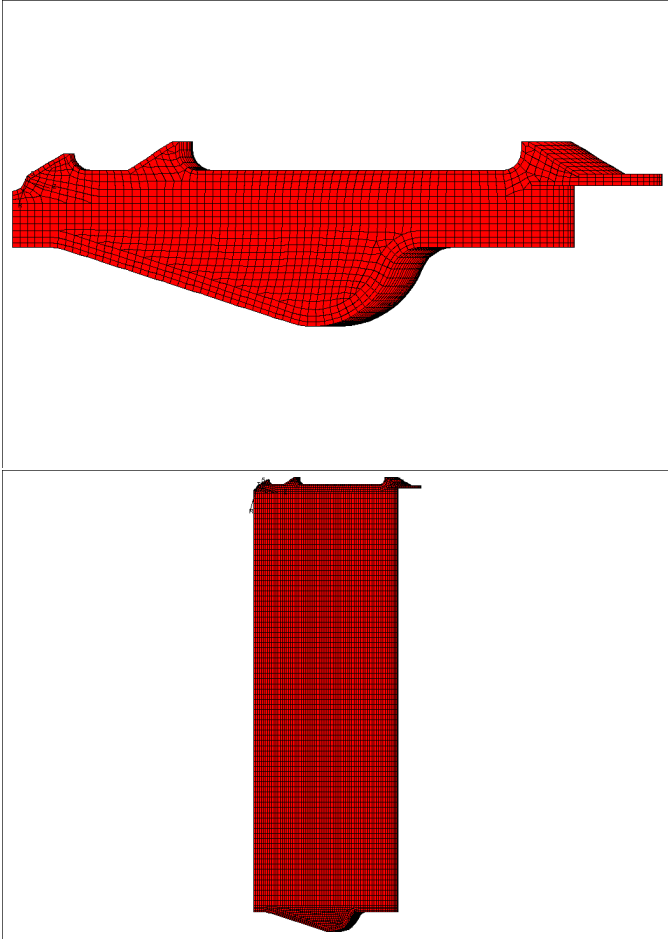


Figure 3: The computational grid used in the simulations, shown at both initial piston position and at crank angle 360°

$$\tau_C = \tau_{ch} + f_{delay}\tau_\epsilon \quad (26)$$

where τ_C is the characteristic time, τ_{ch} is chemical time-scale, f_{delay} is a delay function and $f\tau_\epsilon$ is the turbulent mixing time-scale. The delay function f_{delay} is given as

$$f_{delay} = (1 - e^{-p})/0.632. \quad (27)$$

The term p in the equation above is the ratio of products to the reactive species. The delay function f essentially decreases the influence of turbulent mixing before combustion has started and then allowing it to increase as combustion proceeds.[19]

The reaction rate determined by the characteristic time-scale can be given as

$$\frac{dY_{fuel}}{dt} = \frac{W_l W_t}{W_t + fW_l} \quad (28)$$

where W_l is the chemically limited reaction rate and W_t is the reaction rate limited by turbulent mixing. W_l can be calculated as

$$W_l = A_{ch}[Fuel]^{0.25}[O_2]^{1.5}exp(-E/RT) \quad (29)$$

where A_{ch} is the pre-exponential factor that should be set according to the case, E is the activation energy, T the

temperature and R is the universal gas constant. The reaction rate determined by turbulent mixing is computed from

$$W_t = C_M \rho \frac{\epsilon}{k} \min(m_{Fuel}, \frac{m_{O_2}}{r}) \quad (30)$$

where C_M is a model constant, ρ is the gas density, and r is stoichiometric oxygen to fuel ratio. The constants used for the LaTCT model in the present study are presented in table 3. For comparison also the constants used by Kaario et al. are presented.[19]

Table 3: Model constants used in present study and in study by Kaario et al.

	C_m	A_{ch}	$E(\text{kJ/mol})$
Kaario et al.[19]	3	4000	77.3
Present study	6	8000	77.3

Turbulence A proper choice of turbulence model is very important for the performance of a CFD-model[5]. After testing several different turbulence models the best performance was found with the RNG $k-\epsilon$ model. However it turned out to be necessary to modify the standard model settings in Star-CD in order to get the best performance. The standard RNG $k-\epsilon$ model predicted low cylinder pressures compared to the available experimental data. This was in accordance with the findings of Kaario [19] and the modification of the model parameters suggested in his dissertation, The Influence of Certain Submodels on Diesel Engine Modeling Results, were adopted. The constants used for the turbulence modeling are presented in Table 4.

Table 4: Values for RNG $k-\epsilon$ turbulence model constants

	C_μ	C_1	C_2	C_3	σ_k	σ_ϵ
Std RNG $k-\epsilon$	0.085	1.42	1.68	-0.387	0.719	0.719
Modified RNG $k-\epsilon$	0.085	1.42	1.68	-1.0	0.719	0.719

Atomization and droplet breakup The droplet breakup regime determines the sizes and numbers of droplets produced in the simulation. As every droplet results in a coke particle once all lighter components have evaporated, the atomization and breakup models therefore have a large impact on the particle emissions predicted by the present model. As no detailed experimental data on PM emissions, such as particle size distributions, from the studied case was available, it is difficult to determine the best droplet breakup model to use. The effect of the droplet breakup regime on the PM emissions predicted by the present model and the overall performance of the model is studied by testing two different droplet breakup models in Star-CD. Both models were tested with the standard settings and two sets of modified parameters partly to attempt to achieve optimum performance of the model and partly in order to study the effects of model settings on the results.

Star-CD currently has the following 4 different breakup models available:[22]

- Reitz and Diwakar model
- Pilch and Erdman model
- Hsiang and Faeth model
- KHRT model

The droplet breakup models were often developed to be used with lighter distillate fuels, and it is not therefore clear that optimum performance can be expected from all these models when using HFO as fuel.[5] The viscosity of HFO is often much higher than that of distillate fuels and experiments have shown that viscosity can affect the droplet sizes in a diesel spray.[23] The Weber number is used to determine the breakup regime a droplet experiences. The Weber number is defined as

$$We = \frac{\rho_g u_{rel}^2 D_d}{\sigma_d} \quad (31)$$

where ρ_g is the gas density, u_{rel} is the relative velocity of the droplet, D_d is the droplet diameter and σ_d is the surface tension coefficient. At low Weber number values the droplet stays stable and as the number increases the droplet goes through different breakup modes. Typically low viscosity droplets remain stable when $We < 12$ while higher viscosity droplets can remain stable at higher weber numbers.[23] Ideally the breakup model used in HFO diesel combustion would then both take into account the high viscosity of the fuel and the high Weber numbers encountered in diesel spray combustion.[23] The Hsiang and Faeth model is not valid for high Weber number cases as it lacks a high Weber number breakup regime and is therefore not a good choice for the present case. [23] The Pilch and Erdman model does not consider the droplet viscosity when determining the stable droplet size and is therefore also not an optimal choice for HFO combustion modeling. [23]

The Reitz-Diwakar is the simplest model available for droplet breakup and atomization in Star-CD and where there is lack of more detailed information about the studied spray it is often the best default choice[5]. Additionally while this breakup model is quite simple it does feature a breakup regime for high Weber number conditions and could thus feasibly be applied for diesel combustion processes [23]. Therefore the Reitz-Diwakar model was chosen as a breakup model to be used in this study.

The secondary breakup of droplets is modeled by two droplet breakup regimes:

- Bag breakup
- Stripping breakup

Both regimes have their own criterion for instability and for the characteristic time-scale of breakup.

The Bag breakup process is analogous to the Rayleigh-Taylor instability and is a process where non-uniform pressure around the droplet causes the droplet to deform and ultimately disintegrate as surface tension forces are overcome[5]. In this regime the instability is determined by a critical value of the weber number as follows[22];

$$We \geq C_{b1} \quad (32)$$

where C_{b1} is an empirical coefficient. The associated characteristic time for the droplet breakup is[22]

$$\tau_b = \frac{C_{b2} \rho_d^{1/2} D_d^{3/2}}{4\sigma_d^{1/2}} \quad (33)$$

where C_{b2} is a model constant that is roughly equal to π . Stripping breakup is a process where liquid is stripped off from the droplet surface due to tangential forces[5]. The criterion for the onset of this breakup is[22]

$$\frac{We}{\sqrt{Re_d}} \geq C_{s1} \quad (34)$$

where C_{s1} is a model constant with the value 0.5 and Re_d is the Reynolds number for the droplet which is given as

$$Re_d = \frac{\rho_d u_{rel} D_d}{\mu} \quad (35)$$

where μ is the viscosity of the droplet. The characteristic time-scale for the stripping breakup process is calculated as[22]

$$\tau_b = \frac{C_{s2}}{2} \sqrt{\frac{\rho_d D_d}{\rho_g u_{rel}}} \quad (36)$$

where C_{s2} is a model constant. For both breakup regimes the change in the diameter of unstable droplets is calculated as[22]

$$\frac{dD_d}{dt} = -\frac{D_d - D_{d,stable}}{\tau_b} \quad (37)$$

where $D_{d,stable}$ is the droplet size that satisfies the equality in equations 32 and 34. Garaniya proposed the Reitz-Diwakar breakup model be used with this droplet evaporation subroutine, along with modified parameters that were set to match visual experimental results[5]. The Reitz-Diwakar model settings proposed by Garaniya were tested as an alternative for the standard model settings in Star-CD. Additionally another modified version of the Reitz-Diwakar model was tested, this time with $C_{s2} = 15$, in order to show the effect of this parameter. The three sets constants for the Reitz-Diwakar breakup model that were tested are presented in table 5.

Table 5: Both the standard and modified constants used for the Reitz-Diwakar breakup model

	C_{b1}	C_{b2}	C_{s1}	C_{s2}
Modified R-D[5](Reitz-Diwakar 1)	8.4	0.5	4	26
std. R-D(Reitz-Diwakar 2)	6	0.5	π	20
Modified R-D 2(Reitz -Diwakar 3)	6	0.5	π	15

The Reitz-Diwakar model is not heavily affected by the viscosity of the fuel[23] and therefore it would be interesting to study the importance of the viscosity of the fuel by also testing a model that takes it into account. The KHRT breakup model is affected by droplet viscosity and therefore tests using both the standard settings in Star-CD and a set of alternative parameter values are included in this study. The KHRT model is a hybrid model combining models for Kelvin-Helmholtz (KH) instabilities and Rayleigh-Taylor (RT) instabilities. KH instability is due to aerodynamic forces acting on the droplet surface creating an unstable surface wave and causing liquid to be shed from the surface of the droplet. RT instability is caused by the deceleration of the droplet which causes the droplet to deform and ultimately break into smaller droplets.[22] In the KHRT model these two phenomena compete with each other and the one that predicts the fastest breakup will trigger a breakup event. In the implementation found in Star-CD a KH breakup event will shed mass from the parent parcel and create a new parcel with smaller droplets. The shedding of the child droplets is due to the development of an unstable surface wave and the parent droplet has a diameter larger than the wavelength Λ_{KH} of the wave. The size of the stable child droplets is calculated as

$$D_s = 2B_0\Lambda_{KH} \quad (38)$$

where B_0 is a model constant. The change in size of the parent droplet is calculated in a similar fashion to the Reitz-Diwakar model as

$$\frac{D_d}{dt} = \frac{D - D_s}{\tau_{KH}} \quad (39)$$

where τ_{KH} is the characteristic time for the KH breakup and is given as

$$\tau_{KH} = \frac{3.726B_1D/2}{\Lambda_{KH}\Omega_{KH}} \quad (40)$$

where B_1 is a model constant and Ω_{KH} the growth rate of the fastest growing wave. The criterion for a RT breakup to occur is that that a time longer than the RT breakup time-scale τ_{RT} has passed since the last RT breakup and that the droplet diameter is larger than the wavelength Λ_{RT} of the fastest growing Rayleigh-Taylor wave scaled by a constant C_3 so that[22]

$$D_d > C_3\Lambda_{RT}. \quad (41)$$

The value of Λ_{RT} is obtained by finding the value of the corresponding wave number $k_{RT} = 2\pi/\Lambda_{RT}$ that maximizes the growth rate of the wave calculated as

$$\omega(k) = -k^2\left(\frac{\mu_l + \mu_g}{\rho_l + \rho_g}\right) + \sqrt{k\frac{\rho_l - \rho_g}{\rho_l + \rho_g}a + \frac{k^3\sigma}{\rho_l\rho_g} + k^4\left(\frac{\mu_l + \mu_g}{\rho_l + \rho_g}\right)^2}. \quad (42)$$

The time-scale for RT breakup is then given as

$$\tau_{RT} = \frac{C_\tau}{\omega(k_{RT})} \quad (43)$$

where C_3 is a model constant that is commonly set equal to 1[22]. As can be seen equation 42 contains a term with

the viscosity of the liquid μ_l and thus allows the viscosity of the droplet to influence the breakup due to RT instability. This makes the KHRT model an interesting alternative in HFO simulations as HFO has such a high viscosity[23]. Two sets of parameters for the KHRT model were tested for this study, the standard settings in Star-CD and a set of alternative settings where the settings were modified in order to get the best fit to the experimental data available. The starting point for the modified settings for the KHRT model were the settings found to work best by Bong[23] but a value of 0.4 was used for the constant C_3 instead of the value of 1 suggested by Bong. A third version of the KHRT model was also used with the values of 6 and 0.1 for parameters B_0 and C_3 respectively. This was done to show the effects of changing the value of the C_3 parameter alone. The constants used for the KHRT model in this study are summarized in table 6

Table 6: The constants used for the KHRT breakup model

	C_3	C_τ	B_1	B_0
Std. KHRT(KHRT 1)	0.1	1	0.61	40
Mod. KHRT (KHRT 2)	0.4	1	0.61	6
Mod. KHRT (KHRT 3)	0.1	1	0.61	6

Gas phase soot model In the present study the standard soot model in Star-CD was used with the standard settings. The 4.24 version of Star-CD does offer four alternative soot models but only the one equation laminar flamelet model developed by Mauss et al. was available for the combustion model that was used. This is a simple model that only gives the predicted mass of soot and its spatial distribution in the cylinder as output. It is not possible to get size distributions and the number of particles emitted from this particular model.[22]

Droplet collision and coalescence The droplet evaporation subroutine that is the basis of the present model is not currently compatible with droplet coalescence and thus the collision model in Star-CD was turned off[5].

Solution procedure The PISO solution algorithm with coupled flow Lagrangian multiphase calculations is employed in this study. However as pointed out by Garaniya the droplet mass transfer and droplet properties subroutines used in this study are not compatible with the standard solution procedure for coupled flow[5]. As it was not possible to correct this issue within the scope of this work, the "Predictor only" option was used in the simulations. This provides a faster but somewhat less accurate solution.

Parameters for present model The implementation of the present model into Star-CD includes the creation of 4 fuel components for the droplet. Also the initial amount of each of these component is to be specified. The initial

concentrations of each component are specified in table 7. As can be seen the share of cutter stock was increased from 0.3 to 0.5 while keeping the composition of the cutter stock the same. The increase in the share of the lighter components are partly motivated by the fact that the pressure level results obtained with 0.7 residue share were very low compared to experimental data for the case. Also these parameters should be set to match the fuel that is to be modelled, and based on the information available about the fuel used in the experiments, it is slightly different from the fuel characterized in Garaniya's work. The share of the ratio of cutter stock to residue for the fuel used in the experiments was unknown, but an elemental analysis was available. The HFO sample studied by Garaniya had a sulphur content of 4.5% [5] while the fuel used for the experiments for the studied case had a sulphur content of just 0.5%. Sulphur content can correlate with the content of asphaltenes in the fuel [10] and therefore it was concluded that reducing the amount of heavy residue could give a better approximation of the fuel in this case.

Table 7: The initial fractions of components used in the present model and the model suggested by Garaniya [5]

Component	Present model	Garaniya's model
n-Paraffins	0.25	0.15
Aromatics	0.083	0.05
Naphtenes	0.167	0.1
Residue	0.5	0.7

RESULTS

In the previous sections the implementation of the present model into the CFD code Star-CD 4.24 was described. In this chapter the simulation results will be presented and analysed. The results will be compared to available experimental data, both found in literature and available data from Wärtsilä for the particular case studied here, and the performance of the model will be evaluated. The choice of submodels and parameters will also be motivated and the effects of some of these settings will be studied.

EXPERIMENTAL RESULTS IN LITERATURE Finding suitable experimental results from the literature to evaluate the performance of the present model is quite challenging. The difficulty lies partly in the variation in the results due to differing measurement techniques and partly in the way particle emissions are formed in HFO combustion. Mass flow numbers alone only tell little about the performance of this model as a large amount of the total particle mass can stem from impurities in the fuel, such as ash and sulphur, and the present model is not designed to catch the formation of these. Additionally the present model actually contains two modes for particle formation, both a liquid and gas phase soot model. Therefore more detailed studies about the nature of the PM emitted from HFO combustion are needed in order to distinguish between the different kinds of particle

emissions. Particle size distributions are of interest as well as studies on chemical characterizations of particles of different sizes.

Some studies fulfilling these needs were found in the literature. Moldanová et al. [24] studied the characteristics of PM emitted from a large ship diesel engine using residual oil. They found that the particle size distribution was bimodal with an additional peak in particle mass concentration at around $10\mu\text{m}$ in addition to the fine particle mode typically found in emissions from burning lighter fuel [24]. The findings of Moldanová et al. [24] are in accordance with the findings of Lyyränen et al. [25][26] who also found a peak in particle size distributions in the coarse mode around a particle diameter of about $10\mu\text{m}$ in two separate studies. A study by Fridell et al. [27] also reported a bimodal size distribution with a second coarse mode peak at around $10\mu\text{m}$. Both Fridell and Lyyränen attributed the coarse mode peak partly to re-entrained particles from the combustion system surfaces that have grown through the addition of primary particles [27], [25]. The random nature of inception of re-entrained particles would partly explain the absence of the mode in some measurements [27]. However the mode is also likely partly due to char particles from incomplete combustion of fuel droplets [25].

The larger particles found in the above mentioned studies are generally not reported in studies where particles were studied in ship plumes with for instance aerosol counters. This is likely due to the fact that while larger particles influence the mass flow of PM significantly, they are few in number compared to the small particles that are abundant in emissions from HFO combustion [27].

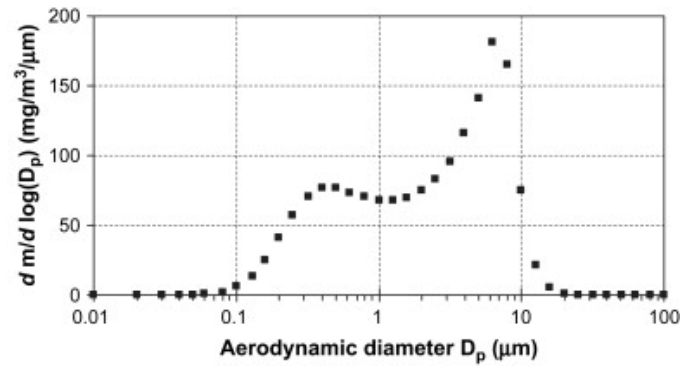
The particle size distributions found in the studies mentioned earlier are presented in Figure 4. As can be seen most curves in Figure 4 show a bimodal distribution with a peak in the coarse mode in addition to the fine particles commonly present in diesel combustion of lighter fuels. Also the presence of particles of all sizes between the two modes can be seen. The particle size distribution measured by Fridell et al. [27] presented in figure 4c also contains a number-size distribution represented by the curve marked N. The number distribution shows that while the coarse mode particles have an influence on the mass of emissions the number of particles in the coarse mode is relatively small compared to the fine mode particles.

When analysing particles in HFO exhaust gases more closely Moldanová et al. identified the following four distinct types of particles: [24]

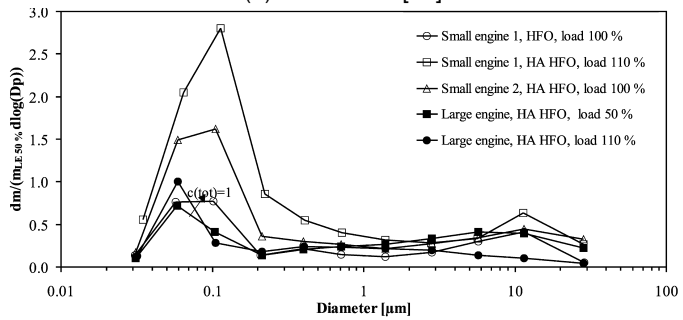
- Soot particles
- Mineral/ash particles
- Organic particles
- Char and Char-mineral particles

Soot particles were found to be small, with a mean size of about 50 nm, and roughly spherical in shape. They are assumed to be nucleated from the volatilized compounds in the fuel and are essentially the emissions modelled by traditional soot models. The soot particles can also form agglomerates of many individual soot particles that can range in size to a few microns.

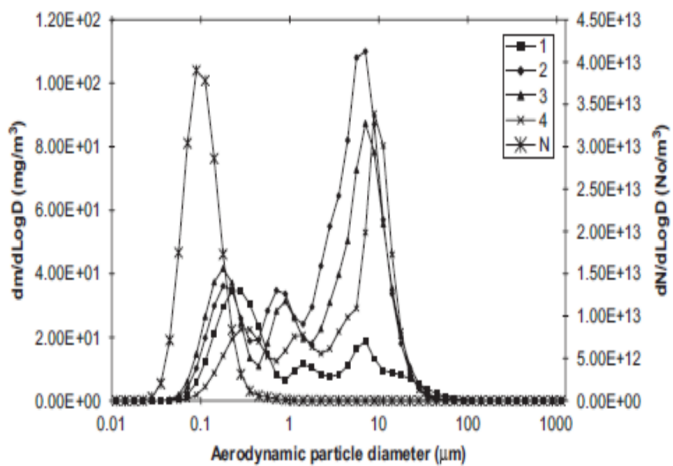
Ash particles originate from the inorganic compounds present in the fuel. As the ash content of HFO is significantly higher than in distillate fuels, the amount of ash particles is also much higher. Ash particles originate from the volatilized inorganic compounds in the fuel and through nucleation form spherical particles of about 40 nm in size [25].



(a) Moldanová [24]



(b) Lyyränen[25]



(c) Fridell[27]

Figure 4: Measured particle size distributions for large marine diesel engines running on HFO found in literature

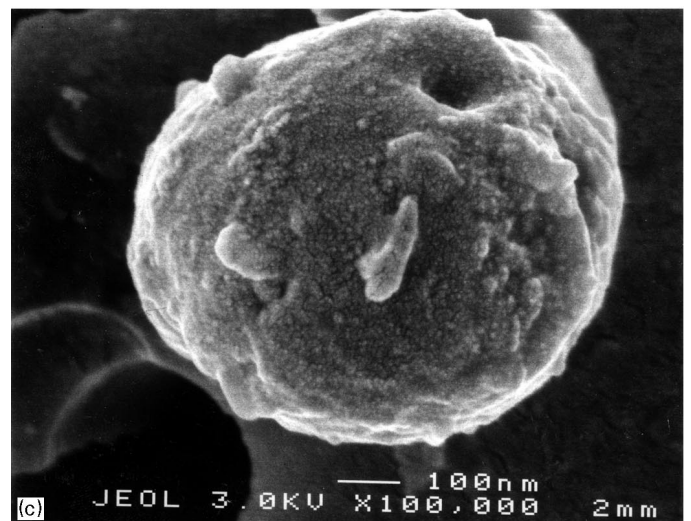
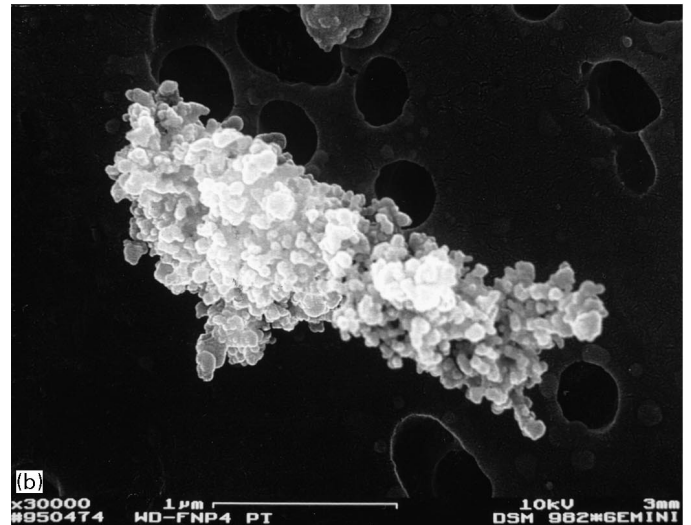
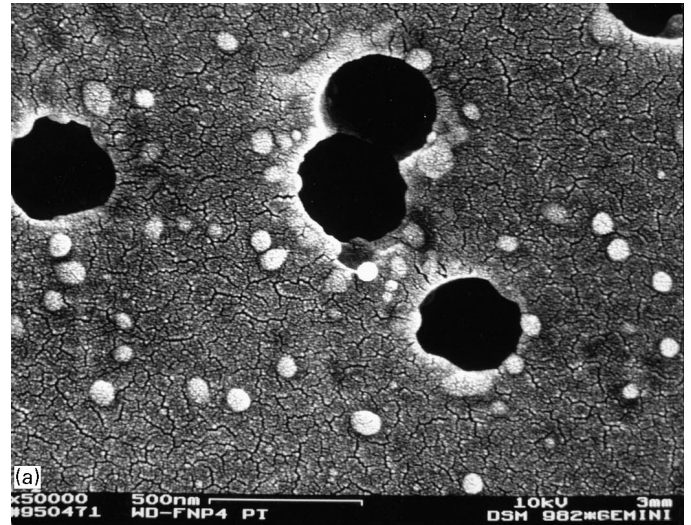


Figure 5: Images of nucleation mode particles(a), agglomerated nucleation mode particles(b) and fuel droplet residue particle(c). Adapted from Lyyränen et. al [25].

The char particles are the group that is of most interest from the point of view of this work. They are assumed to be the residue of the pyrolysis of the heavier compounds

in the fuel droplets and are thus the emission mode modelled by the present model. Moldanová et al. [24] found them to be roughly spherical with sizes ranging from about $0.2\mu\text{m}$ to about $5\mu\text{m}$. Also Lyyräinen et al. [25] reported carbonaceous particles that originated from the residue of fuel droplets. They suggested that they might make a significant contribution to the particles observed between the two main modes, found at $0.1\mu\text{m}$ and $10\mu\text{m}$ [25]. Figure 5 shows images of the particles observed by Lyyräinen et al. [25]. The images clearly show the difference in structure between nucleation mode particles and agglomerations of these and the fuel droplet residue particles which are also known as cenospheres. Although cenospheres are much larger than the nucleated particles, the smaller particles can form agglomerates that are of a similar size as the cenospheres. This makes the differentiation of these different particle emissions difficult even when particle size distributions are known, as there will be some overlap in the particle sizes produced by these two distinct formation mechanisms.

Sarvi et al. studied the chemical composition of PM emitted from a large scale medium speed diesel engine and found that when using HFO the share of carbon in the PM is decreased as load increases. Their hypothesis was that this was due to better burnout of carbon due to better availability of oxygen at high loads [28]. Bartle et al. found that the size distribution of emitted cenospheres seems to depend on the size distribution of droplets in the fuel spray [29]. This supports the fact that each droplet forms an cenosphere. They also found that the asphaltene content of the fuel influenced both the sizes of the droplets and the resulting cenospheres due to its influence on the viscosity of the fuel [29]. Villasenor et al. studied the effects of asphaltenes on HFO droplet combustion and found that while coke formation is not only dependent on asphaltene content of the fuel, high asphaltene content increases the burnout time for created cenospheres [30].

SIMULATION RESULTS In this section the results from the simulations performed for this study are presented. Where possible the results are compared to experimental results from literature in order to evaluate the performance of the present model and to motivate the choices of some submodels and model parameters. As this model gives the opportunity to change the properties of the fuel, the effects of some fuel properties on the results are also examined.

Details about the case As mentioned previously the simulation model used here is based on the Wärtsilä W20 engine. It is an engine with a cylinder bore of 200 mm and a stroke of 280 mm. The diameter of the injector nozzle holes in the case is 0.37 mm. The engine is run at a constant speed of 1000 RPM in all load cases but the duration of fuel injection is different for all three load cases. The times for beginning and end of injection in the simu-

lation model are summarized in table 8. As can be seen

Table 8: Injection duration for each load case

Load	Beginning of injection (CA°)	End of injection (CA°)
100 %	354.611	388.703
50 %	354.708	375.266
10 %	355.012	363.905

injection starts around the same time but the end of injection is at very different times for the three load cases. As the effects of changes to some fuel properties are discussed later in this chapter a summary of the fuel properties used in the following model validation section is in order. The fuel properties used in the simulation model are as follows;

- Viscosity is constant at 0.0135 kg/ms
- Surface tension coefficient is constant at 0.04 N/m
- The density, specific heat and heat of vaporization of the fuel droplets are varied as the composition of the droplet changes
- The initial share of residue component in the fuel is 50 %. More detailed information about fuel composition can be found in table 7

There is experimental data available from test runs with the Wärtsilä W20 engine running on HFO. The available data is mainly average cylinder pressure measurements and this data is used for model validation in the next section.

Model validation As mentioned in earlier sections the present model not only models emissions of particulate matter in a new way but also changes the way fuel properties and droplet evaporation is modelled. This means that in order to get decent performance from this model, settings of a multitude of other submodels also need to be considered, in addition to choosing the proper settings for the evaporation and fuel properties models. Due to the lack of detailed emissions data from the specific case studied it is difficult to establish the optimal model settings to be used for this model when modelling particulate emissions. Instead, attempts have been made to choose model settings in order to model the combustion behaviour according to cylinder pressure as best as possible. This way most submodel settings can be chosen in order to establish a baseline case, to which the effect of altering key model settings and submodels can then be compared. The settings used for the these initial simulations are those described in the previous sections. The droplet atomization model chosen for the baseline case is the modified version of the Reitz-Diwakar model described in Garaniya's work. This was used as reference as it was successfully used in Garaniya's original work with this model.

The average cylinder pressures predicted by the present model are presented in figure 6. The single component mode presented here uses similar sub-model settings as the present multi-component model but uses the standard mass-transfer routine in Star-CD. As can be seen in figure 6a The predicted pressure with the present model is slightly low for the 100 % load case, both with regards to peak pressure and pressure levels during the expansion stroke. The single component model gives a better prediction of pressures in the 100 % case. The low predicted pressures with the present model in the 100 % case are likely due to slower evaporation with this model. Attempts to increase the amounts of fuel vapour and consequently the pressure levels were made by changing the composition of the fuel and speeding up the production of pyrolysis gas by changing the pre-exponential factor for thermal cracking as presented in table 2. As the pressure after these changes, presented in figure 6, is still somewhat low these changes could be considered reasonable.

The pressure predictions for the 50 % load case and the 10 % load case follow the trend of the higher load case in the sense that the predicted pressure for the expansion stroke are a bit too low compared to the experimental data, as can be seen in figures 6b and 6c. The predictions of peak pressure are slightly different as the predicted peak pressure is actually slightly high for the 50 % load case and closer to observed values for the 10 % load case. The model does seem to give reasonable predictions for ignition delay for all the cases.

Although the present model does not perfectly reproduce the pressures found in the experimental data for the case, the performance was deemed to be reasonable. Further optimization of the model could probably result in even better results when it comes to cylinder pressure, but finding better settings to use proved difficult with the data that was available. More detailed data about the fuel used in the experiments could have been helpful for determining the best fuel properties and composition to use. This would then have enabled the optimization work to focus on tuning other submodels for the best performance with these. As there was some uncertainty about the precise nature of the fuel used in the experiments the decision was made to keep the changes to Garaniya's original model settings modest. The performance of the model in the context of pressure predictions was still deemed to be good enough as it is in order to use it to study the emissions of cenospheres, which is the main focus of this study.

Results with standard model settings The predicted particle size distributions for cenosphere emissions are presented in figure 7. As can be seen it would seem that lower loads result in a larger number of smaller particles. Higher loads result in larger particles having a peak in mass concentration at particle diameter of

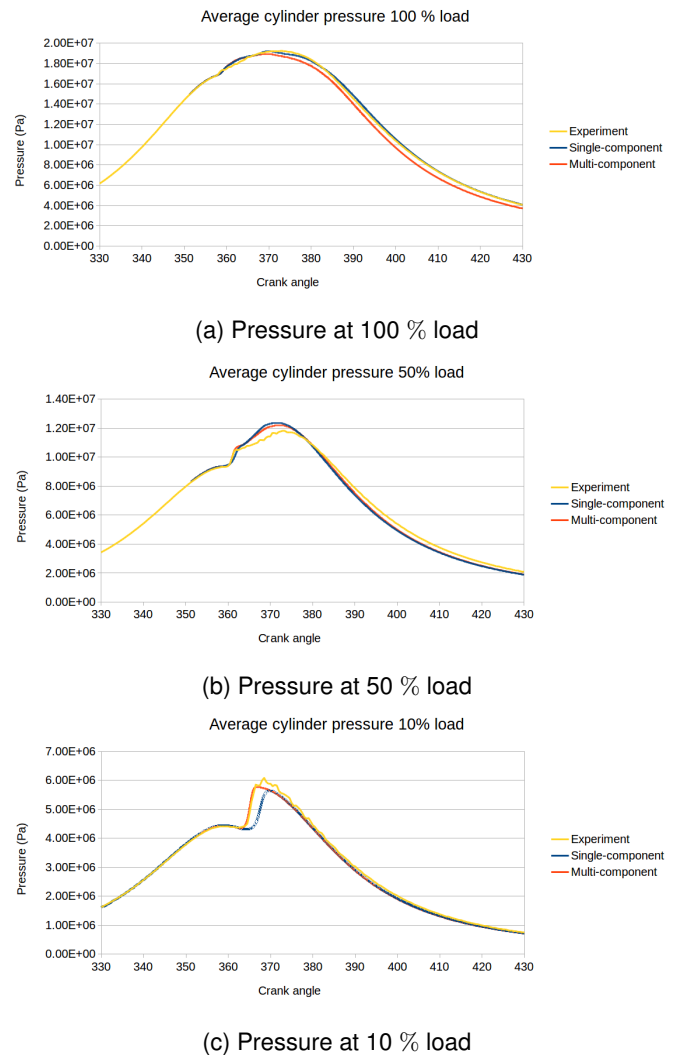
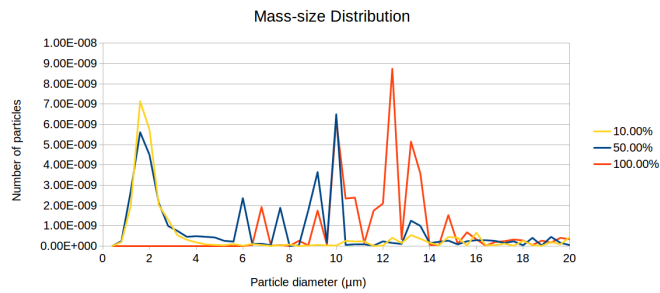


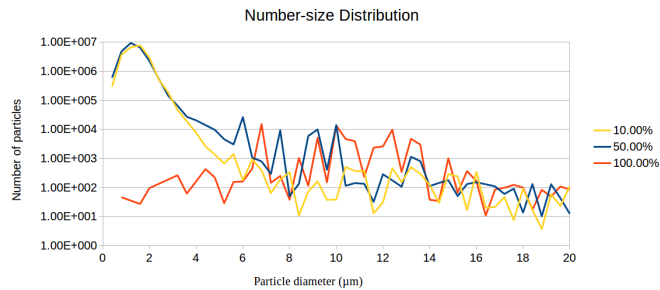
Figure 6: Average pressures at different loads with the present model, a single component model for comparison and according to experimental results for the case.

about 10 μm . The lack of smaller particles at higher loads means that number concentrations are decreased as load increases. As the load decreases the peak in both number and mass concentrations shifts toward smaller particles. It should however be noted that larger particles are also present in the lower load cases, just in significantly smaller numbers than the smaller particles.

The trend of smaller particles with decreasing load is interesting and it is worth studying the reasons behind this. One way to gain insight into the diameters of the emitted cenospheres is to study the evolution of the droplet diameters during the simulation. Figure 8 shows how the sauter mean diameter (SMD) of the droplets changes during the simulation. It can be observed that the evolution of the SMD follows a similar pattern in all three load cases. The diameter initially drops sharply after the start of injection. Then as the injection starts to slow down, the SMD suddenly increases again. After the end of injection the SMD falls once again only to



(a) Predicted mass-size distributions of cenospheres at different loads



(b) Predicted number-size distributions of cenospheres at different loads (note the logarithmic scale on the y-axis)

Figure 7: Particle size distributions for predicted cenosphere emissions

peak again a little later and finally to descend slowly to a plateau. Conclusions that can be drawn from figure 8 are that the large particles found in the 100 % load case are created at the end of the injection and that the average particle size was still decreasing at the end of the simulation in the 100% load case. The slow decrease of the SMD toward the end of the simulation is likely due to the heterogeneous burnout of the cenospheres. The fact that this decrease stops earlier in the lower load cases could be because the low temperature and other conditions cause this reaction to cease earlier during the expansion stroke. As mentioned earlier, the SMD drops initially after the end of injection. This is likely due to droplet breakup, and that the SMD then starts increasing again would be due to the fact that the smallest droplets completely burn out and disappear, which only leaves the larger droplets in the simulation. The higher SMD in the 100 percent load case would then be caused by both large droplets created at the end of injection and better burnout of smaller droplets. The reasons for better burnout of cenospheres in the high load case are both higher temperatures and higher concentration of oxygen in the cylinder during the entire expansion stroke.

The presence of smaller droplets even in the high load case can be confirmed by studying the evolution of the droplet size distributions during the simulation. Figure 9 shows how the droplet size distributions change over time in the high load case. It can be seen that the size distributions remain similar, with a large number of

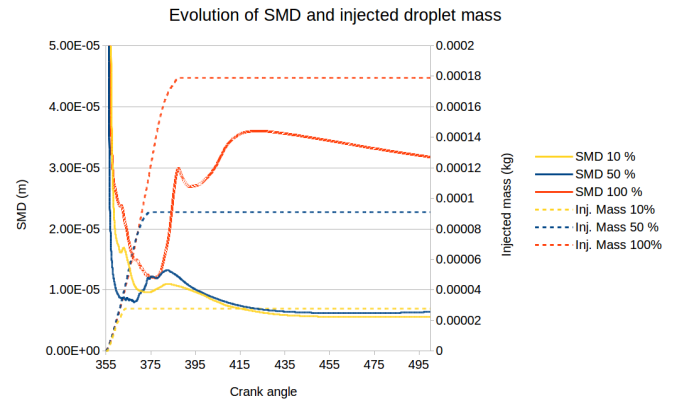


Figure 8: The evolution of the SMD of the droplets and the injected fuel mass during the simulation.

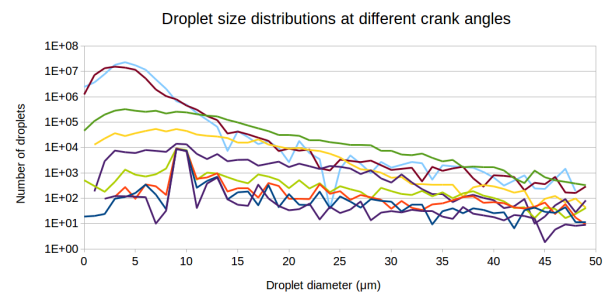


Figure 9: The droplet size distributions at different crank angles for 100 % load case

smaller droplets, under ongoing injection from 370° to 380°. The number of smaller droplets then decrease and there is an increase in larger droplets in the range of about 15 μm to 35 μm as the end of injection is reached at around crank angle 388°. At this point the distribution is quite flat compared to its final form at crank angle 500°, but as the simulation progresses toward its end the droplets smaller than 10 μm are consumed and at a higher rate. Larger droplets break into smaller droplets and thus a peak concentration at about 10 μm is created. As no droplet coalescence model is active the reason for the lack of smaller droplets evaporation, and as the conditions in the high load case are more favourable for evaporation, it makes sense that more of the smallest droplets are consumed than in the lower load cases.

While the total emitted mass in absolute terms from the 100 % case is the highest that does not actually mean much as the higher load naturally means both higher output and higher amount of injected fuel. It is therefore of interest to study the amount of emissions in relation to the injected fuel mass in order to evaluate how emissions at different loads relate to each other. Figure 10 shows the remaining mass of the droplets at the end of the simulation. By this time all lighter components will have evaporated so the leftover droplet mass equals cenosphere emissions. As can be seen the higher load cases give

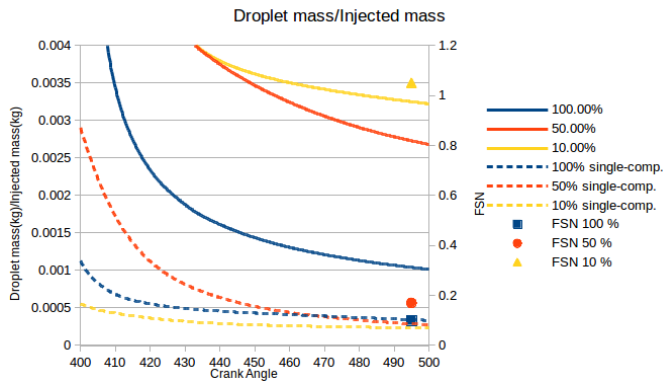


Figure 10: The mass of the remaining particles at the end of the simulation scaled by the mass of injected fuel. Results from single component model included for comparison as well as measured FSN values for the case

lower emissions relative to the amount of injected fuel. This trend mirrors the one predicted by the FSN values, although it should be noted that the correlation between FSN and cenosphere emissions is somewhat unclear. The small amount of unevaporated mass left in the single component case stems from a small number of large droplets left at the end of the simulation.

Effects of secondary droplet breakup model Choosing an appropriate spray breakup model is crucial in any engine simulations. In this case however it is of particular importance as it will directly influence not only the combustion behaviour in the cylinder but also the size-distributions of the particles modelled by the present model. As discussed in previous sections two different spray breakup models were tested with three different sets of parameters for each breakup regime. The breakup models tested in this study were:

- The Reitz-Diwakar model
- The KHRT model

Changing the secondary breakup model will affect more than just the resulting particle size distributions from the simulations. It is therefore of interest to investigate the effect of these changes on the overall combustion behaviour in the model. This can be done by studying the average cylinder pressure predictions obtained with different breakup regimes. These are presented in Figure 11. As can be seen the different settings of the breakup regimes affect the combustion but the differences in the cylinder pressures are not dramatic between the settings chosen for this study.

Without enough detailed data about the cenosphere emissions from the studied case it is not possible to decide which droplet breakup regime works best for this particular case. However trying out different breakup regimes

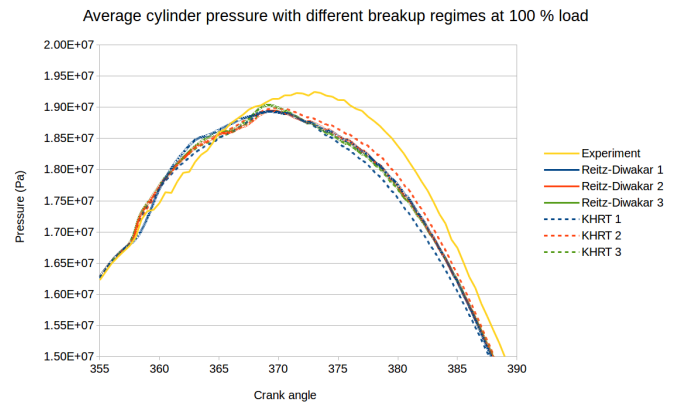


Figure 11: The average cylinder pressures with different breakup regimes at 100 % load

does highlight the differences in results produced by these models. Trying out different parameters on each model gives an understanding of how the parameters change the results and how important optimizing the secondary breakup model parameters is for getting accurate results. The effects of the breakup models on emissions were tested in both the 100 % load case and the 10 % load case. The resulting particle size distributions from these simulations are presented in Figures 12-15. The settings for the different breakup regimes can be found in the Implementation section in the Tables 5 and 6 and the names in the legend of Figures 12-15 correspond to those in the mentioned tables. While the range of droplet sizes presented in the following figures is limited to droplets smaller than $20\mu\text{m}$ it should be noted that larger particles are also present. Numerically they are relatively few but they do make a significant contribution to the total mass flow of PM. The decision to focus on the sub $20\mu\text{m}$ is due to the fact that the peak concentrations do fall within this range as can be seen in Figure 9. Also as far as emissions go the smaller particles are of most interest as they will travel further in the atmosphere, and are also far more abundant in numbers.

It can be observed from Figures 12 and 13 that for the high load case the difference between the Reitz-Diwakar 1 regime, which uses the parameters proposed by Garaniya, and Reitz-Diwakar 2, that is standard version of the model, are quite small. The standard version produces slightly smaller droplets having most droplets in both mass and numbers in droplets with sizes of about $7-11\mu\text{m}$. Garaniya's version of the R-D breakup produced slightly larger droplets, as would be expected due to the higher values in model parameters, with peaks between 10 and $14\mu\text{m}$. In both these cases there was a relatively small number of small particles present. Decreasing the coefficient C_{s2} in the third version of the R-D breakup model resulted in even smaller droplets with mass and number concentration peaks at both $5-7\mu\text{m}$ and below $2\mu\text{m}$.

The standard KHRT model, here named KHRT 1, produced quite similar results to Reitz-Diwakar 1 & 2 with the addition of a smaller peak at below $2\mu\text{m}$. The two

modified versions of the KHRT model produced very few droplets with diameters of below $20\ \mu\text{m}$ compared to the other models. The high peak observed with the KHRT 3 version could be due to some kind of malfunction in the code as the data looked highly irregular. Overall the fast breakup in KHRT 2 & 3 did result in small droplets during the simulation, they were however quickly consumed through evaporation and therefore not present at the end. Both did however produce similar numbers of droplets larger than $20\ \mu\text{m}$ as in the other models.

For the 10 % case all the breakup models resulted in larger numbers of small particles. All the R-D versions produced similar results with most small particles observed with the third version followed by versions 2 and 1 respectively. KHRT versions 1 & 2 also produced high numbers of particles smaller than $2\ \mu\text{m}$ but also had higher numbers of particles present in the $2\text{-}10\ \mu\text{m}$ range which is clearly reflected in the mass distribution presented in Figure 14. Interestingly the KHRT 3 version produced results quite similar to the R-D models.

One conclusion that can be drawn from this comparison of breakup regimes is that all the models seem to preserve the trend of higher numbers of small particles with decreasing load. This would indicate that this is an effect of conditions in the cylinder instead of only a function of different submodel settings. Also it can be concluded that a well functioning droplet breakup model is important for this kind of emissions modelling as there is significant differences between different models and settings, especially between KHRT 2 & 3 and the rest of the models in the 100 % case and KHRT 1 & 2 and the other models in the 10 % case.

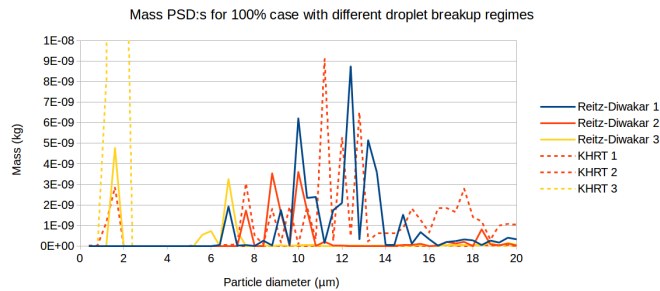


Figure 12: The particle mass size distributions produced by different breakup regimes at 100% load

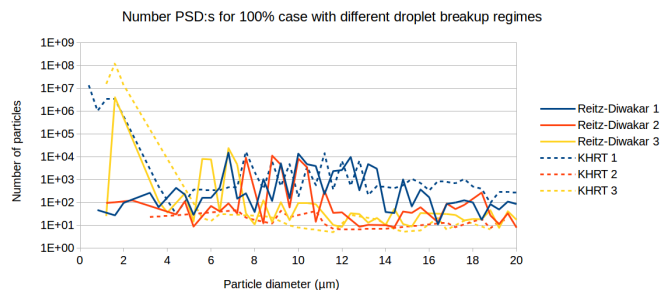


Figure 13: The particle number-size distributions produced by different breakup regimes at 100 % load

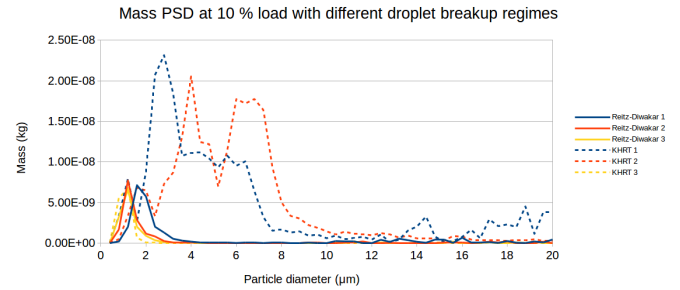


Figure 14: The particle mass-size distributions produced by different breakup regimes at 10 % load

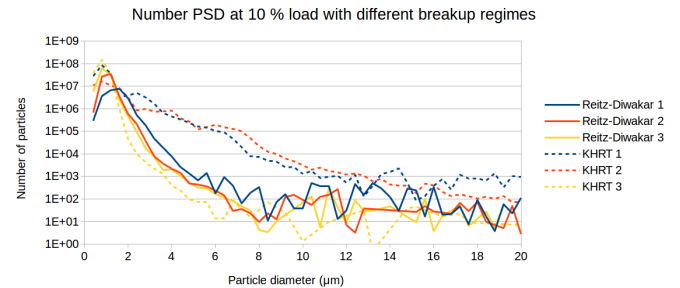


Figure 15: The particle number-size distributions produced by different breakup regimes at 10 % load

Effect of atomization on emissions Changing the parameters of droplet breakup models presents the opportunity to artificially improve the atomization of the spray, leaving all other things the same. This way it is possible to study the effect of decreasing droplet sizes on emissions. The effect of breakup models on size distributions was already presented earlier and here the focus is on studying the effect on particle mass and number flows as atomization is improved.

To study the effect of smaller droplets the cases with Reitz-Diwakar breakup versions 1 and 3 are studied. To demonstrate that the third version of Reitz-Diwakar breakup, described in table 5, actually produces smaller droplets than the first version the SMD of the sprays with both the breakup models are presented in Figure 16. As can be seen Reitz-Diwakar 3 clearly produces smaller droplets.

The effect of spray breakup on emissions can then be seen by comparing the remaining particle mass and numbers in each case. Table 9 shows how decreasing droplet sizes effects emissions of cenospheres. When it comes to mass of emitted particles, improving atomization clearly leads to lower emitted mass. This trend is the same for both load cases studied here. However improving atomization of the spray also leads to an increase in the number of particles emitted. It seems that while improved atomization does improve the burnout of particles, roughly halving the mass emissions of particles depending on the case, the burnout of smaller particles does not completely counteract the increase in

the number of particles the improved atomization causes.

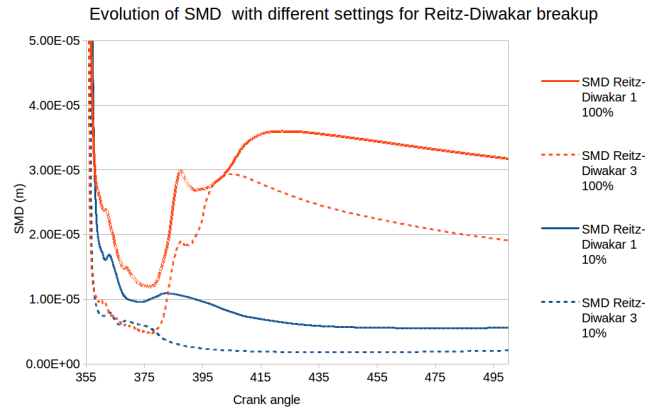


Figure 16: The SMD of droplets produced by variations of the Reitz-Diwakar breakup regime at 100 % and 10 % load

Table 9: The amount of droplets and droplet mass remaining at the end of simulation with different breakup regimes

Case	Total remaining droplet mass (kg)	Total remaining number of droplets
100 % R-D 1	1.82E-07	7.34E+04
100 % R-D 3	1.02E-07	4.03E+06
10 % R-D 1	8.98E-08	2.22E+07
10 % R-D 3	3.90E-08	1.03E+08

Effects of fuel properties One of the interesting opportunities offered by the present model is the possibility to easily change fuel properties and composition. Therefore the effects of some key fuel properties will be examined here.

Viscosity As viscosity is one of the measurable properties used to describe different qualities of HFO and since different HFO:s can have quite different viscosities it is useful to study how sensitive these results are to changes in viscosity. Since the different secondary breakup regimes take the viscosity of the droplets into account in different ways, the effect of viscosity was tested with both the Reitz-Diwakar breakup model and the KHRT model. The results of altering the viscosity of the droplets, presented in Figures 17-20 show that with the Reitz-Diwakar model the effect of viscosity is relatively modest. However with the KHRT model, reducing the viscosity resulted in an significant increase in smaller droplets. This was expected as the two models treat viscosity differently, and point to the fact that if the effect of viscosity on cenosphere emissions is studied the KHRT breakup model should perhaps be preferred. In the present model viscosity is modelled as a constant, but if it was modelled as a function of temperature for instance this could have an effect on the particles predicted by the model, as viscosity does influence atomization of the spray.

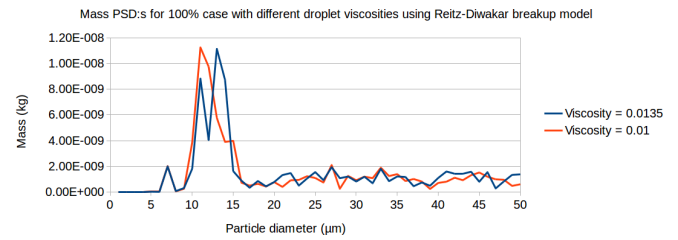


Figure 17: The particle mass-size distributions produced by different viscosities with Reitz-Diwakar breakup regime

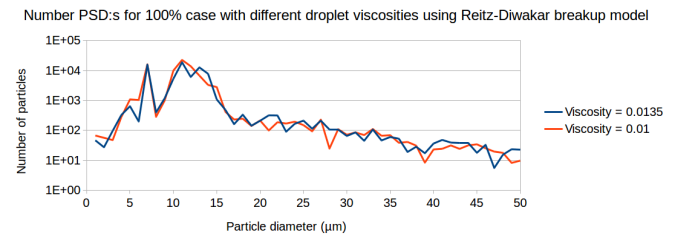


Figure 18: The particle number-size distributions produced by different viscosities with Reitz-Diwakar breakup regime

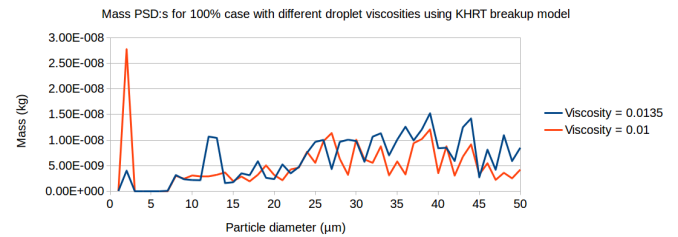


Figure 19: The particle mass-size distributions produced by different viscosities with KHRT breakup regime

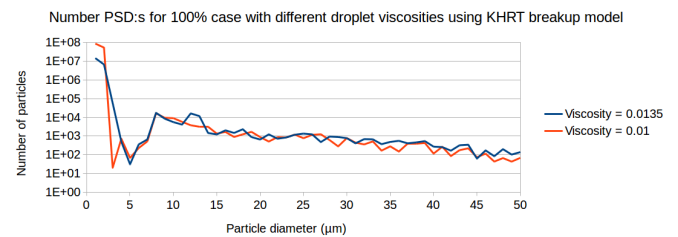


Figure 20: The particle number-size distributions produced by different viscosities with KHRT breakup regime

Fuel composition The present model also gives the opportunity of modifying the composition of the fuel. As many studies have indicated that heavy molecules such as asphaltenes influence the emissions of cenospheres, it is of interest how this model reacts to changes in the amount of the residue component in the fuel. A higher amount of residue should lead to higher emissions. This holds true for the 100% case, presented in Figures 21 and 22, where it can be seen that increasing the amount of residue increases the number of particles emitted. The distribution of the particles is not influenced greatly and

the peak concentrations of mass and number of particles are of similar particle sizes. Figures 23 and 24 show that the same is true for the 10 % load case. The distribution approximately retains its form but the number of particles and mass is increased throughout the range.

The reasons for higher emissions with increased residue are logical. Firstly the residue is the component from which the polymer forming the cenosphere is created and so more of the residue component directly leads to production of more polymer. Secondly increasing the amount of residue makes poorer fuel burn decreasing temperatures in the cylinder and thus possibly slowing down the burnout of cenospheres.

Mass PSD:s for 100% case with different droplet compositions using Reitz-Diwakar breakup model

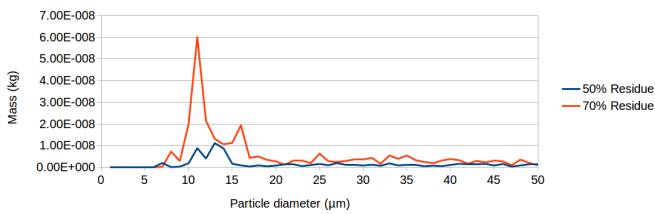


Figure 21: The particle mass-size distributions produced by different fuel compositions with Reitz-Diwakar breakup regime

Number PSD:s for 100% case with different droplet compositions using Reitz-Diwakar breakup model

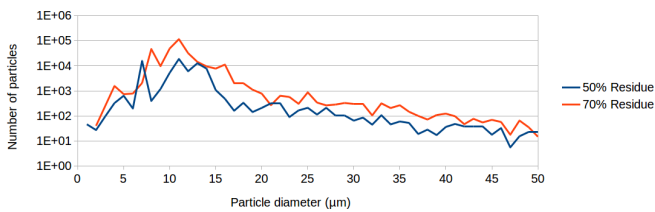


Figure 22: The particle number-size distributions produced by different fuel compositions with Reitz-Diwakar breakup regime

Mass PSD at 10 % load with different droplet compositions with Reitz-Diwakar breakup regime

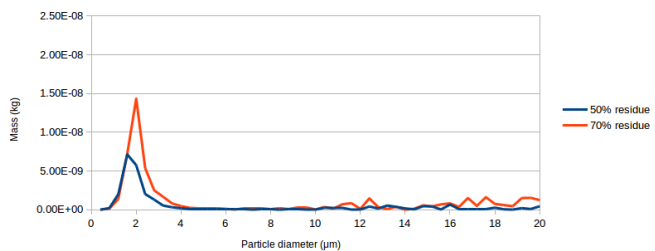


Figure 23: The particle mass-size distributions produced by different fuel compositions for 10 % load case with Reitz-Diwakar breakup regime

CONCLUSIONS

The value of a CFD model is in the conclusions that can be drawn from the results it produces. Therefore the results presented previously are interpreted in this section and the conclusions are evaluated against what is known

Number PSD:s at 10% load with different droplet compositions using Reitz-Diwakar breakup model

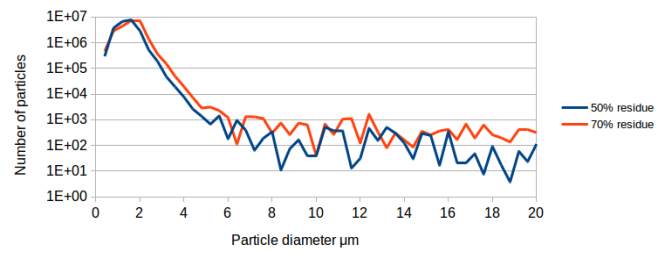


Figure 24: The particle number-size distributions for 10 % load case produced by different fuel compositions with Reitz-Diwakar breakup regime

about the different phenomena from literature. The main conclusions that can be drawn from this model about the behaviour of cenosphere emissions from a diesel engine using HFO are as follows:

1. Size distribution of emitted cenospheres has a correlation to the size distribution of fuel droplets.
2. Increasing the load at same speed (RPM) will decrease the cenosphere emissions relative to fuel consumption.
3. Cenospheres of widely varying sizes are found in emissions and size distributions of cenospheres emitted are dependent on load. At lower loads the highest number of particles are found with a diameter of less than 2 μm while at full load the peak concentration of particles is around 10 μm .
4. Improving atomization of spray will decrease emitted particle mass but may still increase number of emitted particles.
5. Higher viscosity leads to larger particles.
6. Increasing the amount of heavy components in the fuel increases emissions of cenospheres of all sizes.
7. A well working atomization model is important for accurate results

That the size distributions of emitted cenospheres have a correlation to the size distributions of fuel droplets is not surprising as every droplet forms a cenosphere in the present model. The assumption of every droplet forming a cenosphere is supported by the findings of Bomo et al. [4] and could thus be considered reasonable. Bartle et al. [29] also reported a strong similarity between droplet size distributions in the fuel spray and resulting cenosphere emissions. The finding that influencing droplet size distributions influences cenosphere sizes would indicate that emissions of cenospheres could conceivably be influenced by modifying spray atomization.

It was found that improving atomization will decrease emissions of cenospheres, at least in terms of mass

of cenospheres emitted. The finding is not surprising as smaller particles would take less time to burn out, and as burnout of particles is improved, the emissions are naturally lowered. The conclusion that improved atomization will decrease the emissions of particulate mass was also drawn by the modeling studies of Baert and Youan [6][15]. The finding that decreasing the size of the droplets often seems to lead to an increased number of droplets emitted could be a factor to consider if the number of cenospheres, rather than the mass of cenospheres, is of particular concern.

Increasing the viscosity of the fuel increases both the sizes of droplets and the resulting cenospheres. This is not surprising considering the formulations of the droplet breakup models and is also consistent with experimental findings in literature [29]. As the viscosity of the droplets influences atomization, and consequently cenosphere emissions, taking viscosity into account in a reasonable way is important in the present context. Generally viscosity has a tendency to decrease with increased temperature and there are multicomponent evaporation models that model viscosity as a function of temperature available for HFO combustion in context of marine diesel engines [9]. However, as noted by Goldsworthy [7] the preferential evaporation of lighter components will counteract the tendency for viscosity to decrease with temperature due to the highly viscous nature of the residue. Therefore the present model's use of Goldsworthy's assumption of constant viscosity is not completely unreasonable. A model in which viscosity is modelled as a function of both fuel composition and temperature could provide even more accurate results regarding the behaviour of the droplets, compared to the assumption of constant viscosity.

Changing the fuel composition by increasing the share of the residue component in the fuel increases the emissions of cenospheres of all sizes. As discussed earlier this was to be expected and it also agrees with studies in literature which state that poorer quality fuels produce more coke emissions [10][29]. Here the effect of increasing the residue part was studied in an isolated manner without it affecting other fuel properties. In reality increasing the share of residue would affect the viscosity of the droplet and thus the effect on cenosphere emissions could be even more pronounced than observed here [29].

The fact that the emissions relative to injected fuel are diminished as load increases is supported in literature by much data found on emissions from engines. For instance Sarvi et al. observed better burnout of carbon at high loads [28]. Also the higher number concentrations of PM in the 10% in absolute terms compared to the full load case could be consistent with the FSN trend that was available in the experimental data available for the cases. Both the peak concentration of mass at particle sizes of around 10 μm in diameter for the 100 % case and the presence of particles of a wide range of sizes could be considered consistent with the findings of Lyyr nen et al. [25].

Although the present model does seem to react in a reasonable manner according to the results presented above, it is difficult to conclusively validate the performance of the model without more detailed measurement data from the specific case studied here. Accurate measurement data about cenosphere emissions from engines in particular and their dependence on factors such as load would be necessary for accurate calibration of the present model. As such detailed data is not available for the present case, or similar cases in the literature, this study is limited to assessing the performance of the present model through the way the results react to different changes in the simulation, rather than focusing on the specific emission levels. Even if there may be some uncertainty when it comes to the exact emission levels predicted by this model it may however still provide useful information about the formation of these emissions, and the way these emissions are impacted by changes in different operating conditions.

ACKNOWLEDGEMENTS

The presented work has been conducted as part of the HERCULES-2 project within EC's 8th framework programme for research and innovation "Horizon 2020" under grant agreement No. 634135-HERCULES-2.

REFERENCES

- [1] D. Argyros, N. Sabio, C. Raucci, and T. Smith, "Global marine fuel trends 2030," tech. rep., Lloyd's Register Group Limited, UCL Energy Institute, 2014.
- [2] I. Bennett, "Heavy fuel oil combustion; a market segmentation report," tech. rep., TBD Presentations, 2011.
- [3] "Distinctive combustion stages of single heavy oil droplet under microgravity," *Fuel*, vol. 82, no. 3, pp. 293 – 304, 2003.
- [4] N. Bomo, J. Lahaye, G. Prado, and G. Claus, "Twentieth symposium (international) on combustion formation of cenospheres during pyrolysis of residual fuel oils," *Symposium (International) on Combustion*, vol. 20, no. 1, pp. 903 – 911, 1985.
- [5] V. Garaniya, *Modelling of Heavy Fuel Oil Spray Combustion Using Continuous Thermodynamics*. PhD thesis, University of Tasmania, 2009.
- [6] R. Baert, "A mathematical model for heavy fuel droplet vaporization and pyrolysis in a high temperature inert gas," *Combustion Science and Technology*, 1993.
- [7] L. Goldsworthy, "Computational fluid dynamics modelling of residual fuel oil combustion in the context of marine diesel engines," *International Journal of Engine Research*, 2006.

- [8] D. Struckmeier, D. Tsuru, S. Kawauchi, and H. Tajima, "Multi-component modeling of evaporation, ignition and combustion processes of heavy residual fuel oil," *SAE Technical Paper 2009-01-2677*, 2009.
- [9] N. Kyriakides, C. Chryssakis, and L. Kaiktsis, "Influence of heavy fuel properties on spray atomization for marine diesel engine applications," *SAE Technical Paper 2009-01-1858*, 2009.
- [10] H. L. Goldstein and C. W. Siegmund, "Influence of heavy fuel oil composition and boiler combustion conditions on particulate emissions," *Environmental Science Technology*, 1976.
- [11] N. J. Marrone, I. M. Kennedy, and F. L. Dryer, "Coke formation in the combustion of isolated heavy oil droplets," *Combustion Science and Technology*, 1984.
- [12] P. Antaki, "Transient processes in a rigid slurry droplet during liquid vaporization and combustion," *Combustion Science Technology*, 1986.
- [13] A. Lee and C. Law, "Gasification and shell characteristics in slurry droplet burning," *Combust. Flame*, 1991.
- [14] L. W. P. Moszkowicz and G. Claus, "Modelling of very fast pyrolysis of heavy fuel oil droplets," *Chem. Eng. Sci.*, 1996.
- [15] J. Yuan, V. Semiao, and M. G. Carvalho, "Modelling and validation of the formation and oxidation of cenospheres in a confined spray flame," *International Journal of Energy Research*, 1997.
- [16] V. M. Reddy, M. M. Rahman, A. N. Gandhi, A. M. Elbaz, R. A. Schrecengost, and W. L. Roberts, "Cenosphere formation from heavy fuel oil: a numerical analysis accounting for the balance between porous shells and internal pressure," *Combustion Theory and Modelling*, vol. 20, no. 1, pp. 154–172, 2016.
- [17] C. Fink, B. Buchholz, M. Niendorf, and H. Harndorf, "Injection spray analyses from medium speed engines using marine fuels," *ILASS*, 2008.
- [18] D. L. Urban, S. P. Huey, and F. L. Dryer, "Evaluation of the coke formation potential of residual fuel oils," *Symposium (International) on Combustion*, 1992.
- [19] O. Kaario, *The Influence of Certain Submodels on Diesel Engine Modeling Results*. PhD thesis, Helsinki University of technology, Department of Mechanical Engineering, 2007.
- [20] J. Abraham, F. Bracco, and R. Reitz, "Comparisons of computed and measured premixed charge engine combustion," *Combustion and Flame*, 1985.
- [21] S.-C. Kong and R. D. Reitz, "Multidimensional modeling of diesel ignition and combustion using a multi-step kinetics model," *Journal of Engineering for Gas Turbines and Power*, 1993.
- [22] *METHODOLOGY-STAR CD® VERSION 4.24*.
- [23] C. H. Bong, *Numerical and Experimental Analysis of Diesel Spray Dynamics including the Effects of Fuel Viscosity*. PhD thesis, University of Tasmania, 2010.
- [24] J. Moldanova, E. Fridell, O. Popovicheva, B. Demirdjian, V. Tishkova, A. Faccinetto, and C. Focsa, "Characterisation of particulate matter and gaseous emissions from a large ship diesel engine," *Atmospheric Environment*, 2009.
- [25] J. Lyyräinen, J. Jokiniemi, E. I. Kauppinen, and J. Joutsensaari, "Aerosol characterisation in medium-speed diesel engines operating with heavy fuel oils," *Journal of Aerosol Science*, 1999.
- [26] J. Lyyräinen, J. Jokiniemi, and E. Kauppinen, "The effect of mg-based additive on aerosol characteristics in medium-speed diesel engines operating with residual fuel oils," *Journal of Aerosol Science*, 2002.
- [27] E. Fridell, E. Steen, and K. Peterson, "Primary particles in ship emissions," *Atmospheric Environment*, vol. 42, no. 6, pp. 1160 – 1168, 2008.
- [28] A. Sarvi, J. Lyyräinen, J. Jokiniemi, and R. Zevenhoven, "Particulate emissions from large-scale medium-speed diesel engines: 2. chemical composition," *Fuel Processing Technology*, 2011.
- [29] K. Bartle, J. Jones, A. Lea-Langton, M. Pourkashanian, A. Ross, J. Thillaimuthu, P. Waller, and A. Williams, "The combustion of droplets of high-asphaltene heavy oils," *Fuel*, vol. 103, pp. 835 – 842, 2013.
- [30] R. Villasenor and F. Garcia, "An experimental study of the effects of asphaltenes on heavy fuel oil droplet combustion," *Fuel*, 1999.

NOMENCLATURE AND ABBREVIATIONS

SYMBOLS

T_D	Droplet temperature
T_{cr}	Critical temperature
T_{REF}	Reference temperature
R	droplet radius
θ_{Lj}	Mean molecular weight of component j
θ_{jR}	Mean molecular weight of component j at the surface of the droplet
σ_{Lj}^2	Variance of the molecular weight of component j in the liquid phase
σ_{jR}^2	Variance of the molecular weight of component j at the surface of the droplet
γ_j	Distribution origin for the distribution of the molecular weight of component j
ψ_{Lj}	second central moment of the distribution of molecular weight of component j
ψ_{jR}	second central moment of the distribution of molecular weight of component j at droplet surface
α_{Lj}	Shape parameter for distribution for molecular weight of component j in the liquid phase
β_{Lj}	shape parameter for distribution for molecular weight of component j in the liquid phase
y_{FjR}	Concentration of fuel vapour from component j at droplet surface
$y_{Fj\infty}$	Concentration of fuel vapour from component j in surrounding medium, has a value of 0 in this model
R_{GC}	Universal gas constants
P_{atm}	Atmospheric pressure
P_∞	Pressure in the surrounding medium
N	Total molar flux of fuel vapour from droplet surface
ξ_j	Molar flux fraction of component j
Sh_0	Sherwood number for stationary droplet, = 2 in this model
S_{fgj}	Enthalpy of evaporation for component j
D_j	Diffusivity of component j
AR	Aromaticity
B_j	Mass transfer number
E_1	Activation energy
k_1	Pre-exponential factor for reaction rate
E_2	Activation energy
k_2	Pre-exponential factor for reaction rate
E_3	Activation energy
k_3	Pre-exponential factor for reaction rate
E_{poly}	Activation energy
A_{poly}	Pre-exponential factor for polymer
K_c	Chemical rate coefficient
K_d	Diffusion rate coefficient
C_{pLj}	Specific heat of liquid for component j
c	molar density

τ_C	Characteristic time
τ_{ch}	Chemical time-scale
τ_ϵ	Turbulent mixing time-scale
f_{delay}	Delay function in LaTCT model
W_l	Chemically limited reaction rate
W_t	Turbulent mixing limited reaction rate
r	stoichiometric fuel to oxygen ratio in LaTCT model
We	Weber number
Re	Reynolds number

OPERATORS

$\frac{d}{dt}$	derivative with respect to variable t
----------------	---

ABBREVIATIONS

HFO	Heavy Fuel Oil
PM	Particulate matter
CFD	Computational fluid dynamics
IFO	Intermediate Fuel Oil
LCO	Light cycle oil
HCO	Heavy cycle oil
CFI	Coke Formation Index
LAC	Light absorbing carbon
PDF	Probability Density Function
VLE	Vapour-Liquid Equilibrium
LaTCT	Laminar and Turbulent Characteristic time combustion
FSN	Filter Smoke Number
SMD	Sauter Mean Diameter